Optical and Quantum Electronics (2024) 56:1608
https://doi.org/10.1007/s11082-024-07420-5

Optimizing efficiency in CHTS-based solar cells through controlling tin content of (Zn, Sn)O buffer layer and integration of SnS as back surface field layer: a numerical approach

Baseerat Bibi[1] · Tauseef Anwar[2] · Ahmad M. Saeedi[3] · Raed H. Althomali[4] · Gideon F. B. Solre[5] · Sadia Malik[6] · Fatma A. Ibrahim[7] · Mohamed S. Hamdy[7] · Sana Ullah Asif[8] · Waseem Ur Rahman[9] · Saqlain Haider[10]

Received: 31 March 2024 / Accepted: 30 August 2024

Abstract
This study optimizes Cu_2HgSnS_4 (CHTS) solar cells by incorporating a $Zn_{1-x}Sn_xO$ buffer layer and a SnS back surface field (BSF) layer. A detailed numerical analysis was conducted using Solar Cell Capacitance Simulator (SCAPS) software to enhance photovoltaic efficiency. The photovoltaic performance of CHTS-based solar cell CHTS has been evaluated by varying Sn/(Zn+Sn) ratios in the $Zn_{1-x}Sn_xO$ layer, and an optimal ratio of x = 0.31 at the CHTS/ $Zn_{1-x}Sn_xO$ interface is identified, potentially exceeding a 17% efficiency benchmark. Furthermore, strategies to improve open-circuit voltage (V_{OC}) and overall cell performance are investigated, such as modifying the thickness and carrier concentration of the SnS BSF layer. Simulations reveal a significant boost in efficiency, with SnS/CHTS/ $Zn_{0.69}Sn_{0.31}O$ cells reaching an efficiency of 25.81%, surpassing traditional CHTS/CdS cell configurations. Analysis through Capacitance-voltage (C-V) and Mott Schottky plots shows that the optimized cells have low capacitance compared to reference cells, emphasizing the effectiveness of interface and material optimization in enhancing solar cell efficiency. Additionally, impedance spectroscopy analysis highlights the enhanced recombination resistance of the SnS/CHTS/$Zn_{0.69}Sn_{0.31}O$ cells compared to traditional CHTS/CdS cells. These results offer valuable insights into improving the performance of CHTS-based solar cells, significantly contributing to developing sustainable energy technologies.

Keywords CHTS · Back surface field · SCAPS · SnS · Mott Schottky

1 Introduction

The increasing energy demand, combined with the substantial depletion of fossil fuel reservoirs, poses a challenge due to its adverse environmental effects and high production costs. Extensive research endeavors are ongoing to explore alternative energy sources that are sus-

Extended author information available on the last page of the article

Published online: 19 September 2024

tainable, environmentally friendly, and renewable. Solar cell technology emerges as a green alternative to fossil fuels for sustainable energy solutions (Wang and Azam 2024; Kumar et al. 2023). Thin-film solar cells have gained attention due to their cost-effective production, variety of uses, environmental friendliness, improved flexibility and stability, and impressive efficiency (Zhang et al. 2020; Wei et al. 2023; Zhu 2023). Choosing the suitable material is essential when creating solar cells, as qualities like energy band gap, absorption coefficient, exciton binding energy, carrier lifetime, and mobility are vital in determining a material's appropriateness. Metal chalcogenides have emerged as promising candidates for efficient and affordable energy production, providing a reliable and long-lasting option for photovoltaic (PV) technology. Chalcogenides solar cells have reached remarkable efficiencies, such as 23.35% for CIGS (Nakamura et al. 2019), 22.1% for CdTe (Green et al. 2018), and 13 ~ 13.8% for CZTSSe and its Ag-based alloys (Gong et al. 2022; Wang et al. 2018; Baek et al. 2024). Among them, Cu_2ZnSnS_4 is noteworthy because of its resemblance to chalcopyrite and its significance as a solar cell absorber material in single-junction devices. It exhibits a bandgap of 1.5 eV and absorbs light effectively with an absorption coefficient of 10^4 cm^{-1} in the optical range from 826 nm to 250 nm. These characteristics meet the best conditions for solar cell absorbers, as outlined by the Shockley-Queisser limit (Paul et al. 2024; Haddout et al. 2019).

Researchers have been exploring alternatives to Zn in Cu_2ZnSnS_4 due to Cu_{Zn} antisite defects that create a high voltage deficit (Purushotham et al. 2023). These alternatives include substituting Zn with ions like Sr, Ba, Fe, and Hg to eliminate the defects (Crovetto et al. 2019; Ge et al. 2017; Vanalakar et al. 2018; Vu et al. 2019; Bhattacharya et al. 2022). However, these substitutions can impact the bandgap and PV performance. Kukreti et al. introduced CHTS as a promising new absorber material to address this challenge. Through hybrid density functional theory and macroscopic device simulation, they found that CHTS has the potential for over 17% efficiency in solar cells. CHTS presents an exciting alternative for single-junction devices due to its robust absorption coefficient of ~10^4 cm^{-1} (Kukreti et al. 2021). The same research group examined $Cu_2HgSn(S/Se)_4$ in tandem and graded bandgap junction devices. They found that efficiency gains are capped at 17% due to saturation in the bottom sub-cell of tandem configurations (Kukreti et al. 2023). Despite these advances, there is still room for improvement in CHTS-based solar cells, especially in device and interface optimization, to exceed current efficiency benchmarks. Traditionally, CHTS solar cells have used CdS as the heterojunction partner layer. However, CdS is not ideal for long-term commercial applications due to the toxic nature of Cd and associated environmental hazards during production (Jhuma et al. 2019). Additionally, the absorption of sunlight beyond the energy bandgap of CdS (2.4 eV) contributes to optical losses in the shorter wavelength spectrum, thereby diminishing overall efficiency (Bibi et al. 2024). To achieve efficiencies beyond 17% in CHTS solar cells, increasing their V_{OC} by reducing recombination losses is essential, suggesting that the full potential of CHTS in thin-film solar cells has not yet been completely realized.

Different approaches have been suggested to enhance V_{OC} and overall PV performance, including incorporating suitable buffer layers, adjusting band alignment, reducing interface defects, and incorporating a BSF layer. Several studies have demonstrated that the interface recombination rate in solar cells can be reduced by optimizing the conduction band offset (CBO) at the interfaces (Bencherif 2022; Laidouci et al. 2023; Islam and Thakur 2023a, b; Moon et al. 2023; Ahmed et al. 2024). Additionally, buffer layer engineering with ultra-

thin CdS and ZnSnO layers has proven effective for managing the heterojunction interface in flexible CZTSSe solar cells (Xian et al. 2023). ZnSnO, a ternary alloy of ZnO with SnO, shows potential as a substitute buffer layer in CZTSSe solar cells (Zhang et al. 2023). Research conducted by Mukes et al. (Kapilashrami et al. 2012) has demonstrated that higher tin concentration significantly affects the material's band gap, affecting both the valence and conduction bands. Experimental research has shown that the ZnSnO layer can substitute traditional CdS layers to improve solar cell performance by making strategic adjustments to the interface and materials (Hironiwa et al. 2015; Cui et al. 2018; Luo et al. 2022). Back surface recombination hinders the efficiency of solar cells by impeding carrier collection and reducing the device's overall performance (Bibi et al. 2022). Introducing a BSF layer has been recognized as an effective strategy to address this issue. The BSF layer creates a rear pushing force on the highly doped backside of the cell, guiding minority carriers towards the depletion region and passivating the back surface, thereby decreasing rear recombination (Benbouzid et al. 2023). Multiple research studies have shown that tin sulfide (SnS) is effective as a BSF layer in different types of solar cells, including CdTe (Benabbas et al. 2016), Cu_2MnSnS_4 (Isha et al. 2023), and CZTSSe (Gohri et al. 2021). SnS is well-suited for PV applications because it has a high absorption coefficient (105 cm^{-1}) and an optimal bandgap (1.30 eV). Moreover, SnS is plentiful and environmentally friendly, making it a desirable choice for sustainable solar energy technologies (Kuddus et al. 2021).

This study investigates the impact of variations in buffer layer compositions and the integration of a BSF layer on the CHTS solar cell performance. A specific design consisting of Mo/SnS/CHTS/$Zn_{1-x}Sn_xO$/ZnO/AZO layers, with $Zn_{1-x}Sn_xO$ as the buffer layer and SnS as the BSF layer, was employed to investigate their impact on solar cell efficiency. The simulation results showed that adding a $Zn_{0.69}Sn_{0.31}O$ buffer layer enhanced the band alignment at the CHTS/$Zn_{0.69}Sn_{0.31}O$ interface, significantly improving device efficiency. Significantly, the SnS/CHTS/$Zn_{0.69}Sn_{0.31}O$ configuration exhibited an 8% efficiency boost compared to reference CHTS/CdS solar cells, mainly due to a 0.24 V rise in V_{OC}. This study emphasizes the possibility of attaining high efficiency in SnS/CHTS/$Zn_{0.69}Sn_{0.31}O$ solar cells and provides a basis for future research in enhancing CHTS-based PV technologies.

2 Method and material

2.1 Device structure

Figure 1(a) illustrates the schematic of the simulated CHTS-based solar cell structure as described by Sumit Kukreti et al. (Kukreti et al. 2021), which serves as the reference model for this study. The structure includes a window layer of ZnO, a buffer layer of CdS, and an absorber layer of CHTS. Several modifications have been applied to this baseline structure to investigate potential enhancements in device efficiency. Figure 1(b) details the modified configuration, where a ZnSnO buffer layer replaces the traditional CdS buffer layer, and SnS is added as a BSF layer, indicating a strategic alteration aimed at efficiency improvement. The CdS and ZnSnO buffer layers assist in electron transport from the CHTS layer to the external circuit. The ZnO window layer transmits light to the absorber layer, preventing carrier recombination.

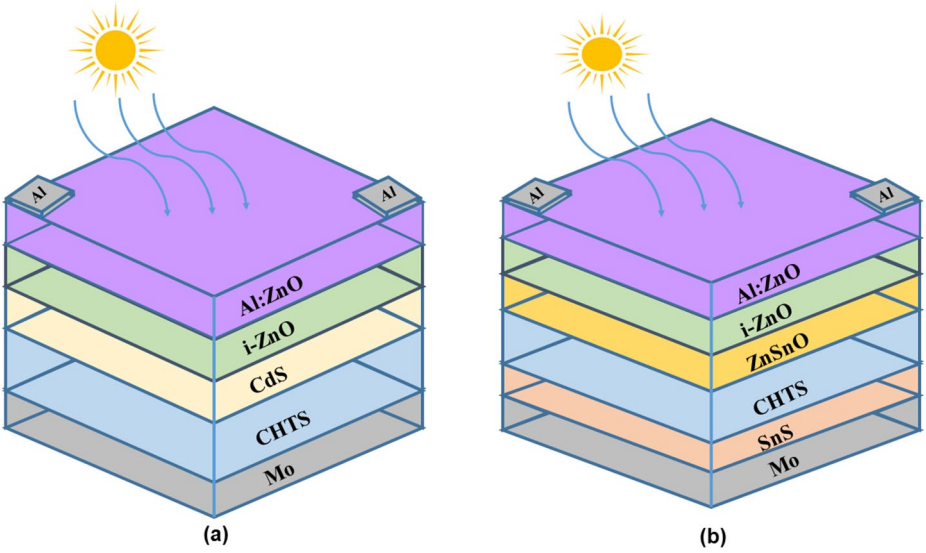

Fig. 1 Configuration of CHTS-based solar cell; (**a**) reference cell featuring a CdS buffer layer, (**b**) optimized cell design incorporating a ZnSnO buffer layer and SnS back surface field layer

2.2 Numerical modeling

Simulation has become essential for analyzing and optimizing conventional thin-film solar cell design and PV performance over the past few decades. In this study, the Solar Cell Capacitance Simulator (SCAPS-1D) developed by the Department of Electronics and Information Systems at the University of Gent examines the CHTS-based solar (Burgelman et al. 2000; Nishat et al. 2021). SCAPS-1D software employs numerical methods to solve one-dimensional semiconductor equations, such as the current density, Poisson, and continuity equations for electrons and holes (Mora-Herrera et al. 2021). The Poisson equation is the fundamental step in obtaining a qualitative understanding of electrostatic variables within a semiconductor, illustrating the relationship between space charges and electrical potential, as shown in Eqs. (1–5).

$$\frac{d^2}{dx^2}\phi\ (x) = \frac{q}{\epsilon_{\ 0}\epsilon_{\ r}}\left(p\,(x) - n\,(x) + N_D - N_A + \rho_{\ p} - \rho_{\ n}\right) \tag{1}$$

Here, φ represents the potential, q the electronic charge, ε the permittivity, n and p the densities of free electrons and holes, respectively, with N_A and N_D indicating the concentrations of ionized donor and acceptor dopants, and ρ_p, ρ_n representing the densities of trapped holes and electrons.

Current conduction in a material involves two primary mechanisms: electric field-induced drift and carrier concentration gradient-driven diffusion. These mechanisms are described by the drift-diffusion equations for solar cells, as outlined in Eqs. (2) and (3).

$$j_n = qD_n\frac{dn}{dx} + q\mu_n nE \tag{2}$$

$$j_p = qD_p\frac{dn}{dx} + q\mu_{\ p} pE \tag{3}$$

The parameters D_n and D_p denote the diffusion coefficients for electrons and holes, respectively, μ_n and μ_p their mobilities, and J_n and J_p the current densities of electrons and holes. The continuity equations consider time-dependent changes such as carrier generation, recombination, and injection at low levels. These equations account for the effects of drift, diffusion, thermal generation, and recombination on carrier concentration changes over time. The continuity equations are expressed as:

$$\frac{d}{dx}j_n(x) - q\frac{\partial n(x)}{\partial t} - q\frac{\partial p_n}{\partial t} = G(x) - R(x) \tag{4}$$

$$\frac{d}{dx}j_p(x) - q\frac{\partial p(x)}{\partial t} - q\frac{\partial n_p}{\partial t} = G(x) - R(x) \tag{5}$$

Applying appropriate boundary conditions at interfaces and contacts leads to a system of coupled differential equations. Solving these equations reveals critical solar cell metrics like the V_{OC}, J_{SC}, FF, and PCE. Furthermore, it facilitates the simulation of I–V, C–V, C–F, and EQE measurements. Recombination dynamics in deep bulk levels are described using the Shockley-Read-Hall (SRH) formalism, and an extension of the SRH formalism captures recombination at interface states.

2.3 Materials properties

The input parameters used in the simulation study are listed in Table 1. Molybdenum (Mo), with a work function (Φ) of 5 eV, serves as the back contact, while Aluminum (Al), having a work function of 4.28 eV, is used for the front contact (Wang et al. 2021). The surface recombination velocity (SRV) for electrons is set at 1×10^5 cm/s; for holes, it is 1×10^7 cm/s for the back contact. While the SRV for electrons is set at 1×10^7 cm/s, and for holes, it is 1×10^5 cm/s for the front contact. The simulation includes critical parameters such as a radiative recombination coefficient of 1×10^{-10} cm^3/s and a capture cross-section of 10^{-15} cm^2 for the CHTS absorber layer. The simulations were performed under AM1.5G solar spectrum conditions, corresponding to a power density of 1000 W/m^2 at a standard temperature of 300 K.

2.4 Establishing the baseline for band alignment: variations in sn content within ZnSnO buffer layers

In advancing the efficiency of PV devices, carefully selecting buffer and absorber layers is a crucial aspect of solar cell engineering. This study focuses on integrating a ZnSnO buffer layer with variable tin (Sn) content, which notably affects band energy dynamics and conduction band offset, both critical factors in device performance. Figure 2(a) illustrates

Table 1 Materials parameters used in the simulation (Kukreti et al. 2021, 2023; Ahmed et al. 2024; Isha et al. 2023; Saadat et al. 2019; Jalali et al. 2023)

Parameters	CHTS	CdS	ZnSnO	i-ZnO	Al: ZnO	SnS
Thickness (μm)	2.00	0.05	0.05	0.08	0.20	0.10
Bandgap (eV)	1.33	2.42	variable	3.30	3.37	1.30
Electron affinity (eV)	4.30	4.5	variable	4.60	4.60	4.20
Dielectric permittivity (εr)	10.60	9.00	9.000	9.00	9.00	12.50
CB effective density of states ($1/cm^3$)	2.20×10^{18}	1.80×10^{19}	3.00×10^{18}	2.20×10^{18}	2.20×10^{18}	1.18×10^{18}
VB effective density of states ($1/cm^3$)	1.80×10^{19}	2.40×10^{18}	1.80×10^{19}	1.80×10^{19}	1.80×10^{19}	4.76×10^{18}
Shallow uniform acceptor density N_A ($1/cm^3$)	1.00×10^{16}	0	0	0	0	1.00×10^{18}
Shallow uniform donor density N_D ($1/cm^3$)	0	1.00×10^{17}	1.00×10^{17}	1.00×10^{17}	1.00×10^{20}	0
Hole thermal velocity (cm/s)	1.00×10^{7}	1.00×10^{7}	1.30×10^{7}	1.00×10^{7}	1.00×10^{7}	1.00×10^{7}
Electron thermal velocity (cm/s)	1.00×10^{7}	1.00×10^{7}	2.40×10^{7}	1.00×10^{7}	1.00×10^{7}	1.00×10^{7}
Hole mobility (cm^2/Vs)	3.50×10^{1}	2.50×10^{1}	4.00×10^{1}	2.50×10^{1}	2.50×10^{1}	1.00×10^{1}
Electron mobility (cm^2/Vs)	1.00×10^{2}	1.00×10^{2}	1.60×10^{2}	1.50×10^{2}	1.50×10^{2}	2.50×10^{1}
Capture cross section electrons (cm^2)	1.00×10^{-15}	1.00×10^{-15}	1.00×10^{-15}	1.00×10^{-15}	1.00×10^{-15}	1.00×10^{-16}
Capture cross section holes (cm^2)	1.00×10^{-15}	1.00×10^{-13}	1.00×10^{-13}	1.00×10^{-15}	1.00×10^{-15}	1.00×10^{-16}
Defect density ($1/cm^3$)	1.00×10^{14}	1.00×10^{14}	1.00×10^{14}	1.00×10^{14}	1.00×10^{16}	1.00×10^{14}

the band alignment of $Zn_{1-x}Sn_xO$, showing the range of bandgap energies varying from 3.3 eV to 2.2 eV with the inclusion of Sn, according to findings reported in (Kapilashrami et al. 2012). The decrease in bandgap observed with higher Sn concentrations in $Zn_{1-x}Sn_xO$ compositions, relative to the ZnO benchmark, is due to the valence band edge (ΔE_v) moving to higher energy levels. Moreover, except for SnO, a moderate elevation in the conduction band edge (ΔE_c) is observed across $Zn_{1-x}Sn_xO$ variants. The introduction of Sn modifies the ZnSnO layer's band energy, thereby influencing the CBO at the CHTS/ZnSnO interface,

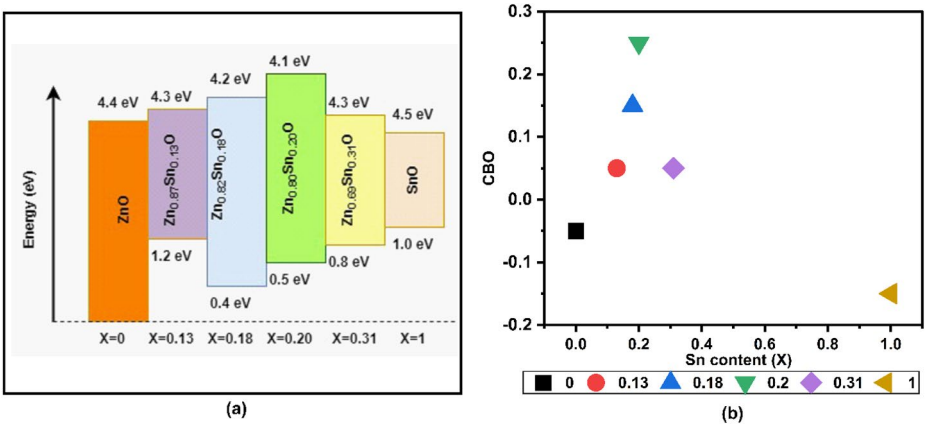

Fig. 2 (**a**) Energy band alignment of ZnSnO alloys with varying Sn content, (**b**) variation in conduction band offset at the CHTS/ZnSnO interface with different Sn content

as illustrated in Fig. 2(b). These offsets are critical as they affect the charge carrier dynamics at the interface, including recombination rates and the effective separation of photogenerated electron-hole pairs. A negative CBO manifests as a "cliff," leading to intensified recombination at the CHTS/buffer interface and diminishing the device's V_{OC} by creating a favorable condition for carrier recombination due to the narrowed energy gap between the buffer's conduction band and CHTS's valence band.

In contrast, a substantial positive CBO greater than 0.3 eV forming a spike shape can impede the photogenerated current in CHTS, thus attenuating efficiency (Gloeckler and Sites 2005). The variation in Sn content aims to alter the buffer layer's properties, optimizing the band alignment with the CHTS absorber. Such alignment is essential for minimizing electron flow barriers, thus improving the solar cell's overall efficiency.

3 Results and discussion

3.1 Verification of CHTS solar cell simulation against literature data

The accuracy of the CHTS solar cell simulation is verified by comparing it with established simulation-based data from the literature. SCAPS 1D was used to replicate the results of Sumit Kukreti et al. (Kukreti et al. 2021)., utilizing CHTS as the absorber layer. The comparison of J-V curves between the current simulation and the Sumit Kukreti et al. (Kukreti et al. 2021) simulation is shown in Fig. 3(a). The computational results yielded a PCE of 10.26%, a V_{oc} of 0.49 V, a fill factor (FF) of 58.30%, and a current density of 35.86 mA/cm², all of which are consistent with the simulation results of Sumit Kukreti et al. (Kukreti et al. 2021). The material properties are presented in Table 1, with the assessment performed at a CHTS defect density of 1E16. Additionally, the quantum efficiency curve of the CHTS/CdS solar cell was obtained during verification. The quantum efficiency of a solar cell measures its effectiveness across different wavelength ranges of sunlight, indicating the cell's sensitivity to particular wavelengths and its performance across the entire light spectrum (Shoab

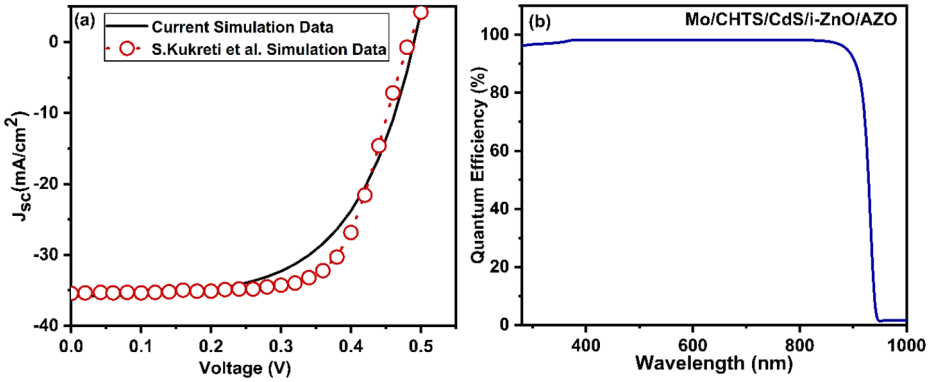

Fig. 3 (**a**) Current simulation J-V curve comparison against literature (Kukreti et al. 2021) and (**b**) Quantum efficiency curve of current simulation

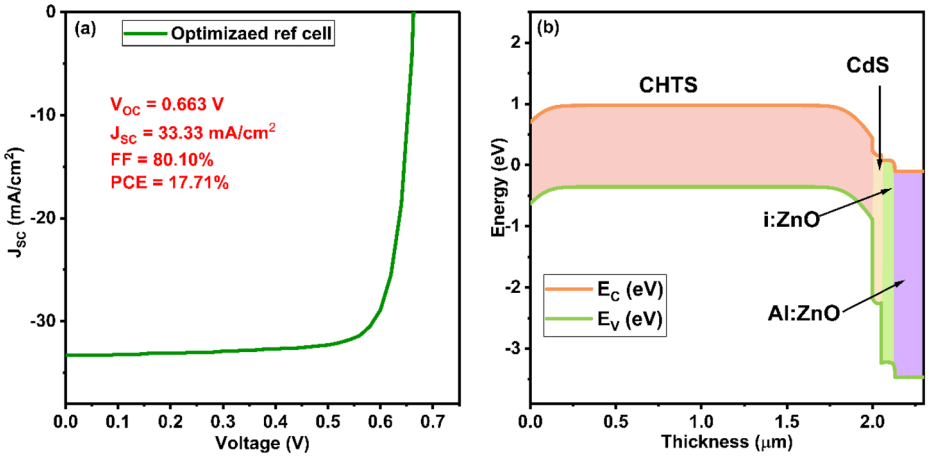

Fig. 4 Photovoltaics performance of simulated reference cell; (**a**) J-V curve, and (**b**) Energy band diagram

et al. 2024). As shown in Fig. 3(b), the quantum efficiency is highest for the wavelength range of 400 nm to 950 nm.

The layer material properties were modified to achieve optimal performance of the reference solar cell. Table 1 represents the optimized material parameters. The J-V curves and energy band diagram of a simulated optimized reference solar cell provide critical insights into its performance and underlying physical mechanisms. The optimized reference solar cell demonstrates reasonable effectiveness with a V_{OC} of 0.633 V, a J_{SC} of 33.33 mA/cm^2, an FF of 80.10%, and a PCE of 17.71%, as shown in Fig. 4(a). However, there is potential for enhancement, particularly in the PCE and V_{OC}. Based on simulation outcomes, the energy band diagram analysis offers a deeper understanding of device performance. Understanding the energy level alignment at the donor-acceptor heterojunction is essential for exploring the solar cell's charge generation and recombination dynamics (Li et al. 2046; Zhu et al. 2024; Bai et al. 2022). As depicted in Fig. 4(b), the simulation reveals that the E_C of the

CHTS absorber layer is positioned higher than that of the CdS layer, resulting in a CBO of -0.2 eV that forms a cliff-like barrier. Such a steep CBO can increase the likelihood of carrier recombination at the absorber/buffer interface, potentially impacting the device's efficiency (Mora-Herrera et al. 2021; Sekar et al. 2023).

3.2 Enhancing CHTS solar cell efficiency through buffer layer tuning

A $Zn_{1-x}Sn_xO$ buffer layer was introduced to address the issue discussed in Sect. 3.1, resulting in a more favourable junction at the CHTS/$Zn_{1-x}Sn_xO$ interface. The simulation identified an optimal tin (Sn) content in the $Zn_{1-x}Sn_xO$ layer, with x representing the ratio of [Sn] to the sum of [Zn] and [Sn], effectively tuning the CBO at the CHTS/ $Zn_{1-x}Sn_xO$ junction. Based on the experimental and simulation data, the Sn content were set at 0.13, 0.18, 0.20, 0.31, and 1.0 for the CHTS/ $Zn_{1-x}Sn_xO$ heterojunction configuration (Saadat et al. 2019; Lee et al. 2018). The influence of varying Sn content within the $Zn_{1-x}Sn_xO$ buffer layer on the CHTS solar cells' performance was extensively analyzed, as shown in Fig. 5(a, b). It was observed in Fig. 5(a) that the V_{OC} peaked at x = 0.2, corresponding to a high positive CBO of 0.25 eV. However, other performance parameters, particularly efficiency, were reduced.

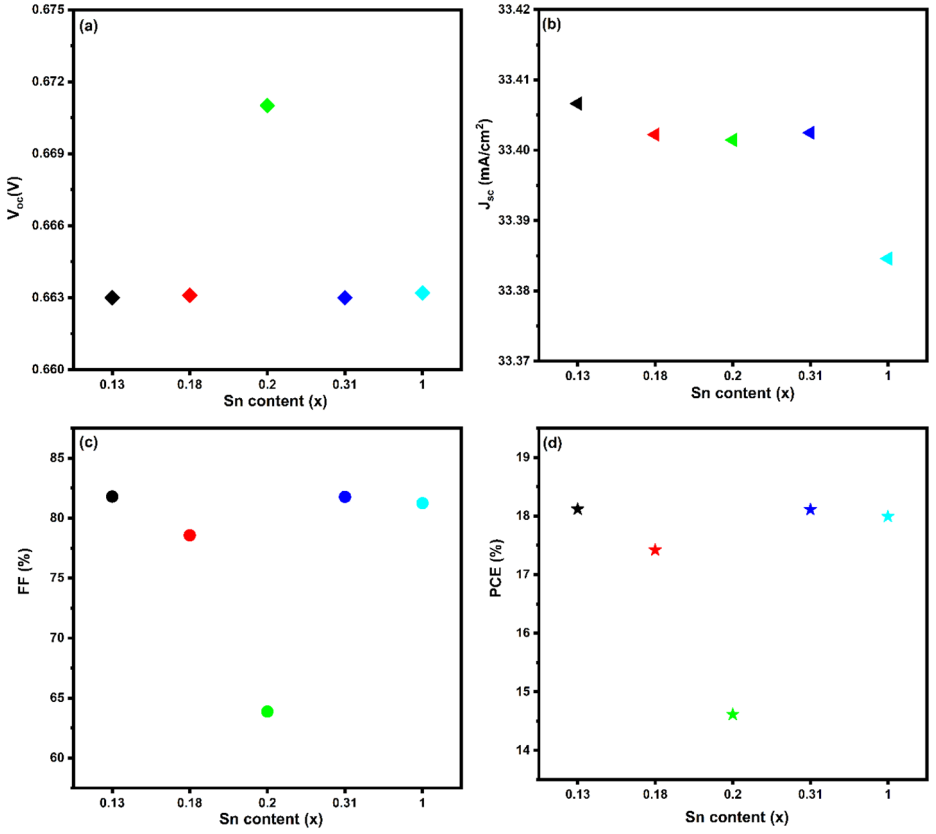

Fig. 5 Photovoltaic parameters of CHTS/$Zn_{1-x}Sn_xO$ solar cells with different tin content: (**a**) $V_{OC,}$ (**b**) $J_{SC,}$ (**c**) FF, (**d**) PCE

The high positive CBO at the buffer/absorber interface can enhance V_{OC} by reducing recombination losses, but it can also decrease the fill factor by increasing series resistance and hindering electron transport due to the formation of a strong barrier (Yadav et al. 2024). Figure 5(b) shows that the maximum J_{SC} was achieved with an x value of 0.31, indicating an optimal bandgap of the buffer layer that minimizes optical losses. Figure 5(c) demonstrates that the maximum value of FF is achieved at x = 0.31, attributed to reduced resistance losses, encompassing shunt and series resistances (Bagade et al. 2023). The findings suggest that the solar cell exhibits the highest efficiency at an x value of 0.31, demonstrating the beneficial impact of adjusting the composition of the $Zn_{1-x}Sn_xO$ buffer layer on enhancing solar cell efficiency.

Figure 6(a) presents the J-V characteristics of the optimized heterostructure, consisting of Mo/CHTS/$Zn_{0.69}Sn_{0.31}O$/ZnO/AZO/Al, where a significant increase in the J_{SC} from 33.24 mA/cm² to 33.40 mA/cm² is observed. The FF also increases from 80 to 82%, resulting in an overall device efficiency increase from 17.59 to 18.12%. The enhanced performance is attributed to the optimal CHTS/$Zn_{0.69}Sn_{0.31}O$ interface, facilitating better band alignment, reduced recombination rates, and decreased optical loss due to E_g expansion in the buffer layer compared to the optimized reference cell. The depicted band alignment at the CHTS/ $Zn_{0.69}Sn_{0.31}O$ interface, detailed in Fig. 6(b), features a minimal spike-like CBO of +0.05 eV or presents an almost flat band scenario. The strategic formation of a spike structure at the interface acts as a barrier to mitigate interface recombination, thereby increasing the cell's efficiency (Lin et al. 2023). These insights affirm the ability to fine-tune the conduction band offset of CZTSSe/$Zn_{1-x}Sn_xO$ by carefully adjusting the Sn/(Zn + Sn) ratio. The alignment of energy bands at the heterojunction interface is a critical factor in the material selection, especially when replacing toxic CdS buffer layers. Further enhancements to the optimized CHTS/$Zn_{0.69}Sn_{0.31}O$ solar cell design are explored by introducing a SnS BSF layer in subsequent analyses.

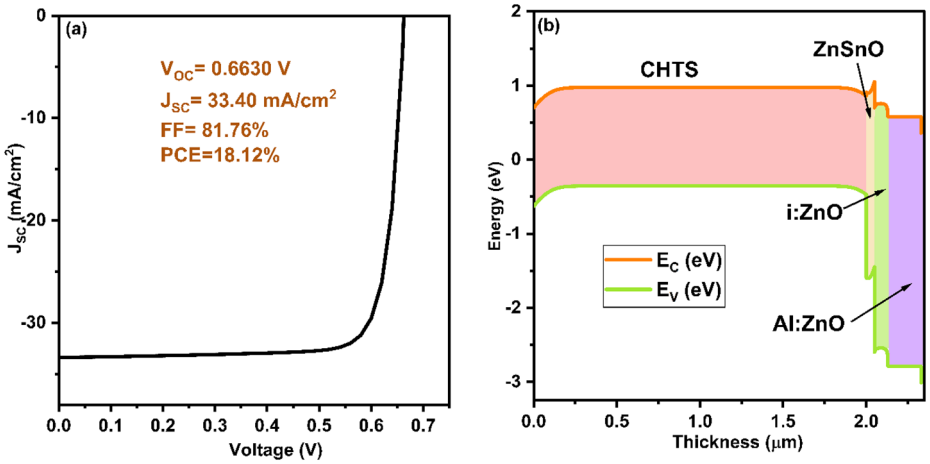

Fig. 6 Photovoltaic performance of CHTS/$Zn_{0.69}Sn_{0.31}O$ solar cell; (**a**) J-V curve, and (**b**) Energy band diagram

3.3 Optimization of thickness and carrier concentration of SnS back surface field layer

The efficacy of BSF layers in boosting the performance of solar cells has been recognized within the PV research community for decades. The BSF layer introduces an additional built-in electric field, oriented in the same direction as that generated by the p-n junction, thus facilitating an increase in the solar cell's V_{OC} (Mondal et al. 2023; Verma et al. 2021). Additionally, the BSF layer supplements the built-in electric field and is pivotal in diminishing the diffusivity and conductivity of minority carriers (electrons) near the back contact (Karade et al. 2022). Figure 7(a, b) illustrates the PV performance of a SnS/CHTS/$Zn_{0.69}Sn_{0.31}O$ solar cell, examining the influence of the SnS BSF layer's thickness at a constant acceptor concentration of 1×10^{18} cm^{-3}. As shown in Fig. 7(a), the J-V characteristics underscore the significant influence of the BSF layer's thickness on the device's performance metrics. Notably, both the J_{SC} and V_{OC} experience substantial increases from 33.62 mA/cm^2 to 34.82 mA/cm^2 and from 0.78 V to 0.87 V, respectively, as the thickness of the BSF layer is increased, reaching a saturation point for thicknesses beyond 0.1 µm. The observed enhancement in J_{SC} and V_{OC} with increased BSF layer thickness indicates a reduced recombination rate of photogenerated carriers within the cell's active region (Islam et al. 2023). However, as the SnS BSF layer thickness increases, there is a decrease in the FF due to increased series resistance and decreased electric field strength (Islam and Thakur 2023a, b). Despite these challenges, the overall PCE exhibits a positive trend with increased SnS BSF layer thickness as shown in Fig. 7(b).

Figure 7(c) illustrates the variation in quantum efficiency as a function of light wavelength for different thicknesses of the SnS BSF layer. Quantum efficiency measures the ratio

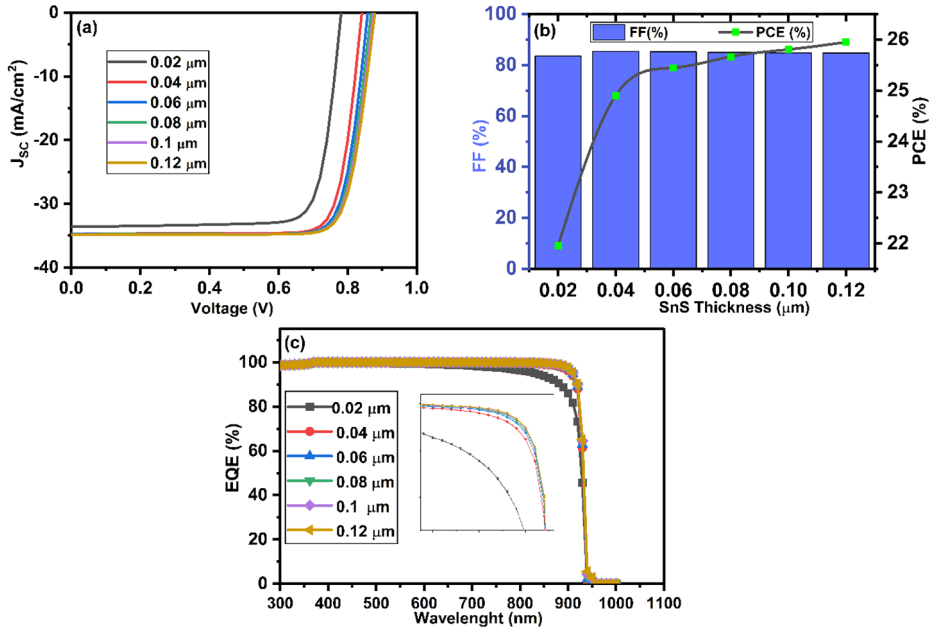

Fig. 7 Effect of the thickness of the SnS BSF layer on the photovoltaic parameters of CHTS/$Zn_{0.69}Sn_{0.31}O$ solar cell; (**a**) J-V curve, and (**b**) FF and PCE (**c**) Quantum efficiency curve

of charge carriers generated by incident light to the number of photons incident on the solar cell (Jahan et al. 2024). Initially, quantum efficiency increases with the SnS BSF layer's thickness, reaching an optimal point beyond which further increases in thickness result in no significant change. As shown in the inset of Fig. 6c, quantum efficiency increases when the thickness is augmented from 0.02 µm to 0.1 µm. However, beyond this point, the quantum efficiency plateaus indicate that additional thickness increases do not substantially enhance the photocurrent.

Figure 8 illustrates the significant impact of the SnS BSF layer acceptor concentration on the PV parameters of SnS/CHTS/$Zn_{0.69}Sn_{0.31}O$ heterostructure solar cells. The carrier concentration within the BSF layer plays an essential role in determining the magnitude and distribution of the electric field, which in turn affects the device's efficiency. Increasing the BSF layer's acceptor concentration enhances the electric field, improving carrier collection and overall device performance (Mohanty 2021). The J-V curves in Fig. 8(a) show the effects of various acceptor concentrations. The V_{OC} increases from 0.72 V to 0.87 V as the SnS acceptor concentration rises from 1×10^{15} cm^{-3} to 1×10^{18} cm^{-3}.

Additionally, there is a slight increase in the J_{SC} from 33.49 mA/cm^2 to 34.82 mA/cm^2. Figure 8(b) explores the impact of the acceptor concentration of the SnS BSF layer on the FF and PCE. It is noticed that the FF improves significantly from 82.51 to 84.74% when the acceptor concentration is increased from 1×10^{15} cm^{-3} to 1×10^{18} cm^{-3}. Correspondingly, the PCE also improves from 19.80 to 25.81% with the increase in acceptor concentration. The higher acceptor concentration in the BSF layer reduces the reverse saturation current, improving the device's performance (Dakua et al. 2024).

3.4 Capacitance–voltage and Mott–schottky characteristic of solar cell

The capacitance-voltage (C-V) characteristics play a critical role in understanding the fundamental aspects of solar cells. The C-V curve, closely linked to the built-in voltage (V_{bi}), offers insights into the solar cells' loss mechanisms. This analysis is demonstrated by comparing C-V characteristic curves and Mott-Schottky plots between a reference CHTS/CdS and optimized SnS/CHTS/$Zn_{0.69}Sn_{0.31}O$ solar cells, as presented in Fig. 9(a, b). The capacitance of a p-n junction changes with applied voltage, affecting the depletion region's width at the material interface. With an increase in voltage, the depletion region narrows, leading

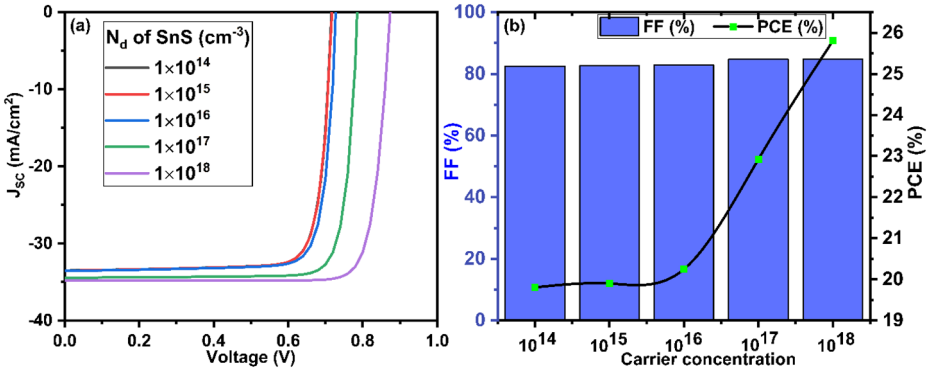

Fig. 8 Effect of different SnS BSF layer acceptor concentrations on the photovoltaic parameters CHTS/$Zn_{0.69}Sn_{0.31}O$ solar cell; (**a**) J-V curve, and (**b**) FF and PCE

to a rise in capacitance (Jili et al. 2023). The Mott-Schottky plot is essential for determining the V_{bi}, which is crucial for directing photogenerated carriers toward their respective terminals, enhancing the solar cell's efficiency. The Mott-Schottky formula is giver by (Wang et al. 2019):

$$\frac{1}{C^2} = \frac{2\epsilon_{r,p}N_A + \epsilon_{r,n}N_D)(V_{bi} - V)}{qA^2\epsilon_0\epsilon_{r,p}\epsilon_{r,n}N_AN_D} \tag{6}$$

C represents capacitance, A is the area, ε the permittivity of free space, q is the electron charge, N_A and N_D are the acceptor and donor concentration, V_{bi} is the built-in potential, and V is the applied voltage.

Equation (6) illustrates that an increase in capacitance inversely affects the V_{bi}. However, a higher V_{bi} is beneficial as it lowers the recombination rate, improving the solar device's efficiency. The analysis of simulated C-V characteristics for the reference and optimized cells, as shown in Fig. 9(a), reveals that the reference cell exhibits higher capacitance. Figure 9(b) illustrates the inverse relationship between V and the capacitance squared (C^2). The V_{bi} can be determined by extrapolating the $1/C^2$ V plot, which correlates with the depletion region's width. The intersection of the extrapolated reference and optimized solar cell graph with the voltage axis typically represents the V_{bi} in the devices. By comparing the optimized SnS/CHTS/ $Zn_{0.69}Sn_{0.31}O$ configuration to the CHTS/CdS structure, which has a V_{bi} of 0.67 V, the optimized configuration has a superior V_{bi} of 0.88 V, indicating an enhancement in the V_{OC}.

3.5 Nyquist plots of solar cell

Impedance spectroscopy is a pivotal technique extensively utilized in the solar cell domain. The comparative analysis of Nyquist plots for reference CHTS/CdS and optimized SnS/CHTS/$Zn_{0.69}Sn_{0.31}O$ heterostructures, facilitated through SCAPS-1D simulation, delves into the junction quality within solar cells, offering an intricate evaluation of their characteristics. The simulations, depicted in Fig. 10(a, b), involve applying a minor AC voltage fluctuation across a spectrum of frequencies at a predetermined DC bias voltage, enabling

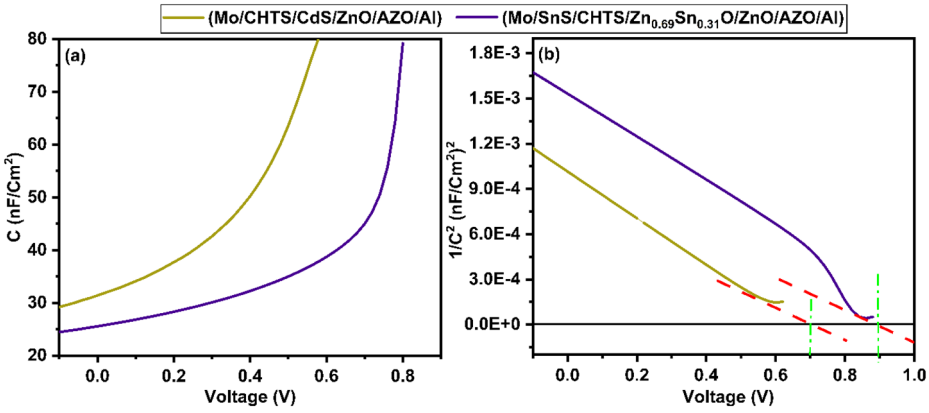

Fig. 9 Comparison of the optimized solar cell; (**a**) capacitance-voltage curves and (**b**) Mott-Schottky curve with reference cell

the calculation of impedance (Z) at each frequency from the resultant AC response. The real (Z′) and imaginary (Z′′) impedance components are obtained, depicted on a Nyquist plot with Z′ along the x-axis and -Z′′ on the y-axis. An equivalent circuit model, detailed in the inset of Fig. 10(a), is adapted to fit the simulated data points, enabling the extraction of series resistance (R_S) and recombination resistance (R_{rec}) values from the plot. R_{rec} signifies the cell's charge recombination resistance, inversely related to its recombination rate.

Conversely, R_S denotes the cell's series resistance, which includes the cell's intrinsic resistance and the resistance in the electrical contact. The analysis reveals that the optimized SnS/CHTS/ $Zn_{0.69}Sn_{0.31}O$ solar cell exhibits a notably larger semicircle diameter, indicative of a superior R_{rec} and, consequently, a diminished recombination rate relative to the reference CHTS/CdS solar cell. A heightened R_S value on a Nyquist plot signals increased resistance within the circuit, potentially curtailing the cell's overall efficiency. The values of R_S and R_{rec} are shown by the plot intersections with the x-axis at low and high frequencies, respectively (Ishaq et al. 2018). The SnS/CHTS/$Zn_{0.69}Sn_{0.31}O$ cell's superior recombination resistance underscores a more efficient p-n junction, illustrating its capability to reduce electron capture by defect traps and minimize interface recombination, thereby boosting efficiency.

3.6 Optimized CHTS-based solar cell

The optimal parameters were determined by selecting the optimal buffer layer and determining the best conditions for the thickness and carrier concentration of the BSF layer. As shown in Fig. 11(a, b), the J-V and quantum efficiency curves of the optimized SnS/CHTS/ $Zn_{0.69}Sn_{0.31}O$ solar cell configuration significantly improve compared to the optimized CHTS/CdS reference cell configuration. Table 2 summarizes the electrical parameters of the optimized SnS/CHTS/$Zn_{0.69}Sn_{0.31}O$ cell solar cell and the reference CHTS/CdS solar cell, highlighting the benefits of the proposed cell design in improving efficiency through optimized electrical properties.

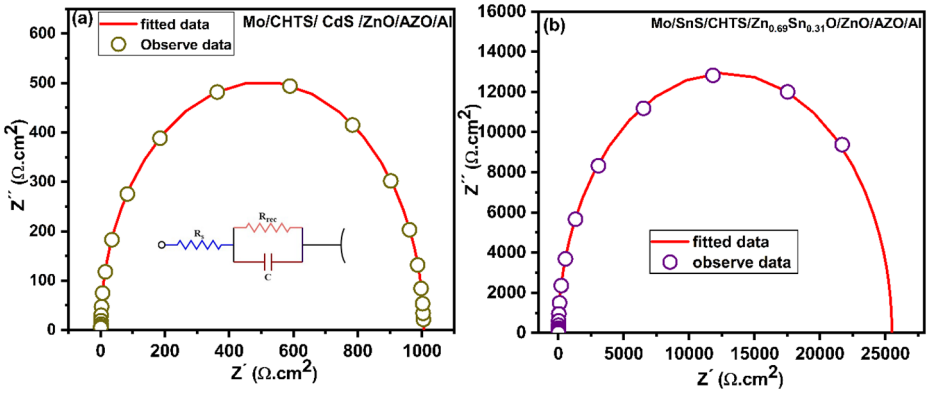

Fig. 10 Simulated Nyquist curves; (**a**) reference cell, (**b**) optimized solar cell

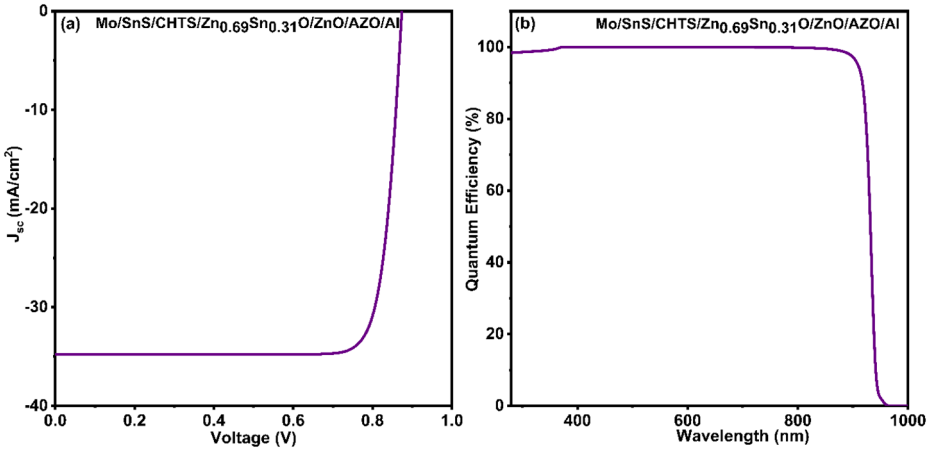

Fig. 11 Optimized CHTS-based solar cell; (**a**) J-V, (**b**) Quantum efficiency curve

Table 2 Comparison of the optimized solar cell photovoltaic parameters with reference solar cell

Structure of solar cell	PCE (%)	J_{SC} (mA/cm^2)	V_{OC} (V)	FF (%)	V_{bi} (V)	R_s (Ω/cm^2)	R_{sh} (Ω/cm^2)
CHTS/CdS	17.71	33.33	0.663	80.10	0.67	0.758	1004
SnS.CHTS/ZnSnO	25.81	34.83	0.874	84.74	0.88	0.14	25,500

4 Conclusion

This study presents the development and performance evaluation of SnS/CHTS/ZnSnO heterojunction solar cells intending to achieve high efficiency. The study highlights the advantages of a (Zn, Sn)O buffer layer over traditional CdS, particularly in band alignment tuning. By adjusting the Sn content in the $Zn_{1-x}Sn_xO$ (x = 0.31) buffer layer, an optimized solar cell with a maximum efficiency of 18.12% was developed. Implementing a highly doped thin p+-SnS BSF in the CHTS/$Zn_{0.69}Sn_{0.31}O$ solar device significantly enhances the efficiency by up to 25.81% and V_{OC} by approximately 0.874 V. Advanced simulation analyses, employing both Mott-Schottky and impedance spectroscopy, provided compelling evidence that replacing the conventional CdS buffer with a $Zn_{0.69}Sn_{0.31}O$ layer and the addition of SnS as a BSF layer not only elevates the built-in potential but also effectively reduces recombination at the junction, leading to a notable improvement in overall cell performance. Ultimately, this research introduces an innovative SnS/CHTS/$Zn_{0.69}Sn_{0.31}O$ solar cell configuration that achieves an unprecedented efficiency of 25.81%, substantially surpassing the benchmark efficiency of about 17% for the reference CHTS/CdS solar cell. Such advancements highlight the potential of this new solar cell configuration in enhancing the efficiency and sustainability of solar energy technologies, marking a pivotal step forward in renewable energy research.

Acknowledgements The Authors extend their appreciation to the Deanship of Scientific Research at King Khalid University for funding this work through Large Groups Project under grant number (RGP2/106/45).

Author contributions The Author, B.B., and W.R., suggest the idea. B.B., S.U.A., W.R., and T.A. optimized the properties of the material. R.H.A., A.M.S., S.M., F.A.I., G.F.B.S., S.H., and M.S.H., analyzed the data.

Authors M.S.H. and S.U.A. helped to write the initial draft and helped to improve the manuscript till the final version. The manuscript was written through the contributions of all authors. All authors have approved the final version of the manuscript.

Funding The Authors extend their appreciation to the Deanship of Scientific Research at King Khalid University for funding this work through Large Groups Project under grant number (RGP2/106/45).

Data availability No datasets were generated or analysed during the current study.

Declarations

Ethical approval We, the undersigned, declare that this manuscript is original, has not been published before, and is not currently being considered for publication elsewhere. We confirm that the manuscript has been read and approved by all named authors and that there are no other persons who satisfied the criteria for authorship but are not listed. We further confirm that all have approved the order of authors listed in the manuscript us.

Competing interests The authors declare no competing interests.

References

Ahmed, T., Islam, M.C., Pappu, M.A.H., Mostaque, S.K., Mondal, B.K., Hossain, J.: A highly efficient n-CdS/p-Ag2S/p+-SnS thin film solar cell: Design and simulation. Eng. Rep., p. e12849, (2024)

Baek, M.C., et al.: Achieving highly efficient kesterite solar cells using simultaneous surface Ge substitution and rear interface engineering strategies. Chem. Eng. J. **479**, 147842 (2024)

Bagade, S.S., Barik, S.B., Malik, M., Patel, P.K.: Impact of band alignment at interfaces in perovskite-based solar cell devices, *Materials Today: Proceedings*, (2023)

Bai, X., Xu, M., Li, Q., Yu, L.: Trajectory-battery integrated design and its application to orbital maneuvers with electric pump-fed engines. Adv. Space Res. **70**(3), 825–841 (2022)

Benabbas, S., Rouabah, Z., Bouarissa, N., Chelali, N.: The role of back surface field SnS layer in improvement of efficiency of CdTe thin film solar cells, *Optik*, vol. 127, no. 15, pp. 6210–6217, (2016)

Benbouzid, Z., Benstaali, W., Rahal, W.L., Hassini, N., Benzidane, M.R., Boukortt, A.: Efficiency enhancement by BSF optimization on Cu (In1 – x, Gax) Se2 solar cells with tin (IV) sulfide buffer layer. J. Electron. Mater. **52**(7), 4575–4586 (2023)

Bencherif, H.: Towards a high efficient Cd-free double CZTS layers kesterite solar cell using an optimized interface band alignment. Sol. Energy. **238**, 114–125 (2022)

Bhattacharya, A., Mishra, V., Tkachuk, D.G., Mar, A., Michaelis, V.K.: Mercurial possibilities: Determining site distributions in Cu 2 HgSnS 4 using 63/65 Cu, 119 sn, and 199 hg solid-state NMR spectroscopy. Phys. Chem. Chem. Phys. **24**(39), 24306–24316 (2022)

Bibi, B., Farhadi, B., Asghar, H.N.U.H.K., Rahman, W.U., Liu, A.: Effect and optimization of the Zn3P2 back surface field on the efficiency of CZTS/CZTSSe tandem solar cell: A computational approach. J. Phys. D. **56**(2), 025502 (2022)

Bibi, B., Farhadi, B., Rahman, W.U., Liu, A.: Numerical modeling and performance analysis of a novel Cd-free all-kesterite tandem solar cell using SCAPS-1D. Next Mater. **2**, 100068 (2024)

Burgelman, M., Nollet, P., Degrave, S.: Modelling polycrystalline semiconductor solar cells. Thin Solid Films. **361**, 527–532 (2000)

Crovetto, A., et al.: Wide band gap Cu2SrSnS4 solar cells from oxide precursors. ACS Appl. Energy Mater. **2**(10), 7340–7344 (2019)

Cui, X., et al.: Enhanced heterojunction interface quality to achieve 9.3% efficient Cd-free Cu2ZnSnS4 solar cells using atomic layer deposition ZnSnO buffer layer. Chem. Mater. **30**(21), 7860–7871 (2018)

Dakua, P.K., Panda, D.K., Kashyap, S., Laidouci, A., Sadanand: Simulation and numerical modeling of high-efficiency CZTS solar cells with a BSF layer. Int. J. Numer. Modelling: Electron. Networks. **37**(2), e3188 (2024). Devices and Fields

Ge, J., et al.: Oxygenated CdS buffer layers enabling high open-circuit voltages in earth-abundant Cu2BaSnS4 thin-film solar cells. Adv. Energy Mater. **7**(6), 1601803 (2017)

Gloeckler, M., Sites, J.: Efficiency limitations for wide-band-gap chalcopyrite solar cells. Thin Solid Films. **480**, 241–245 (2005)

Gohri, S., Madan, J., Pandey, R., Sharma, R.: Performance analysis for SnS-and Sn2S3-based back surface field CZTSSe solar cell: A simulation study. J. Electron. Mater. **50**(11), 6318–6328 (2021)
Gong, Y., et al.: Elemental de-mixing-induced epitaxial kesterite/CdS interface enabling 13%-efficiency kesterite solar cells. Nat. Energy. **7**(10), 966–977 (2022)
Green, M.A., Hishikawa, Y., Dunlop, E., Levi, D., Hohl-Ebinger, J., Ho-Baillie, A.: WY Solar cell efficiency tables (version 51). Prog Photovoltaics Res. Appl. **26**(1), 3–12 (2018)
Haddout, A., Raidou, A., Fahoume, M.: A review on the numerical modeling of CdS/CZTS-based solar cells. Appl. Phys. A. **125**, 1–16 (2019)
Hironiwa, D., et al.: Annealing effect on Cu2ZnSn (S, Se) 4 solar cell with Zn1–xMgxO buffer layer. Phys. Status Solidi (a). **212**(12), 2766–2771 (2015)
Isha, A., et al.: High efficiency Cu2MnSnS4 thin film solar cells with SnS BSF and CdS ETL layers: A numerical simulation, *Heliyon*, vol. 9, no. 5, (2023)
Ishaq, M., et al.: Efficient double buffer layer Sb2 (SexS1–x) 3 thin film solar cell via single source evaporation. Solar RRL. **2**(10), 1800144 (2018)
Islam, M.T., Thakur, A.K.: Design Simulation of Chalcogenide Absorber-Based Heterojunction Solar Cell Yielding Manifold Enhancement in Efficiency, *physica status solidi (a)*, vol. 220, no. 23, p. 2300290, (2023a)
Islam, M., Thakur, A.: Multistep design simulation of heterojunction solar cell architecture based on SnS absorber. Phys. Scr. **98**(10), 105950 (2023b)
Islam, M.C., Mondal, B.K., Ahmed, T., Pappu, M.A.H., Mostaque, S.K., Hossain, J.: Design of a highly efficient n-CdS/p-AgGaTe2/p+-SnS double-heterojunction thin film solar cell. Eng. Res. Express. **5**(2), 025056 (2023)
Jahan, N., et al.: A comparative study of CuO based solar cell with ZnTe HTL and SnS2 ETL using SCAPS 1D simulation. J. Opt. pp. 1–13, (2024)
Jalali, H., Orouji, A.A., Gharibshahian, I.: Controlled conduction band offset in Sb2Se3 solar cell through introduction of (Zn, Sn) O buffer layer to improve photovoltaic performance: A simulation study. Sol. Energy Mater. Sol. Cells. **260**, 112492 (2023)
Jhuma, F.A., Shaily, M.Z., Rashid, M.J.: Towards high-efficiency CZTS solar cell through buffer layer optimization. Mater. Renew. Sustainable Energy. **8**, 1–7 (2019)
Jili, N., Dlamini, N., Mola, G.T.: Computational investigation of the effect ZnS buffer layer on the hole transport of polymer solar cell. Phys. B: Condens. Matter. **666**, 415122 (2023)
Kapilashrami, M., et al.: Soft X-ray characterization of zn 1−x sn x O y electronic structure for thin film photovoltaics. Phys. Chem. Chem. Phys. **14**(29), 10154–10159 (2012)
Karade, V.C., et al.: Combating open circuit voltage loss in Sb2Se3 solar cell with an application of SnS as a back surface field layer. Sol. Energy. **233**, 435–445 (2022)
Kuddus, A., Mostaque, S.K., Hossain, J.: Simulating the performance of a high-efficiency SnS-based dual-heterojunction thin film solar cell. Opt. Mater. Express. **11**(11), 3812–3826 (2021)
Kukreti, S., Gupta, G.K., Dixit, A.: Theoretical DFT studies of Cu2HgSnS4 absorber material and Al: ZnO/ZnO/CdS/Cu2HgSnS4/Back contact heterojunction solar cell. Sol. Energy. **225**, 802–813 (2021)
Kukreti, S., Sapkota, D.J., Dixit, A.: Designing Graded Band gap active layer Cu2HgSn (S1–x Se x) 4 over Complex Tandem Structure for Efficient Photovoltaic Cells with efficiency > 20%. Energy Fuels. **37**(16), 12335–12344 (2023)
Kumar, C.M.S., et al.: Solar energy: A promising renewable source for meeting energy demand in Indian agriculture applications. Sustain. Energy Technol. Assess. **55**, 102905 (2023)
Laidouci, A., Singh, V., Dakua, P.K., Panda, D.K.: Performance evaluation of ZnSnN2 solar cells with Si back surface field using SCAPS-1D: A theoretical study, *Heliyon*, vol. 9, no. 10, (2023)
Lee, S., Kim, S., Shin, S., Jin, Z., Min, Y.-S.: Band structure of amorphous zinc tin oxide thin films deposited by atomic layer deposition. J. Ind. Eng. Chem. **58**, 328–333 (2018)
Li, X., et al.: Mapping the energy level alignment at donor/acceptor interfaces in non-fullerene organic solar cells, *Nature Communications*, vol. 13, no. 1, p. 2022. (2046)
Lin, B., et al.: Efficient Cd-Free flexible CZTSSe solar cells with Quality interfaces by using the Zn1–x sn x O buffer layer. ACS Appl. Energy Mater. **6**(2), 1037–1045 (2023)
Luo, Y.-D., et al.: Energy band alignment for Cd-free antimony triselenide substrate structured solar cells by co-sputtering ZnSnO buffer layer. Sol. Energy Mater. Sol. Cells. **240**, 111721 (2022)
Mohanty, B.C.: Improving performance of Cu2ZnSnS4 solar cell via back contact interface engineering. Sol. Energy. **230**, 986–995 (2021)
Mondal, B.K., Mostaque, S.K., Hossain, J.: Unraveling the effects of a GeSe BSF layer on the performance of a CuInSe 2 thin film solar cell: A computational analysis. Opt. Continuum. **2**(2), 428–440 (2023)
Moon, M.M.A., Biplab, S.R.I., Ali, M.H., Rahman, M.F., Rana, M.S., Kuddus, A.: Computational investigation of Zn-based single buffer layers toward Cd-free high-efficiency CIGS thin film solar cells. J. Appl. Sci. Eng. **26**, 1799–1808 (2023)

Mora-Herrera, D., Pal, M., Santos-Cruz, J.: Theoretical modelling and device structure engineering of kesterite solar cells to boost the conversion efficiency over 20%. Sol. Energy. **220**, 316–330 (2021)
Nakamura, M., Yamaguchi, K., Kimoto, Y., Yasaki, Y., Kato, T., Sugimoto, H.: Cd-free Cu (in, Ga)(Se, S) 2 thin-film solar cell with record efficiency of 23.35%. IEEE J. Photovolt. **9**(6), 1863–1867 (2019)
Nishat, S.S., et al.: Performance analysis of perovskite solar cells using DFT-extracted parameters of metal-doped TiO2 electron transport layer. J. Phys. Chem. C. **125**(24), 13158–13166 (2021)
Paul, R., et al.: Recent progress in CZTS (CuZnSn sulfide) thin-film solar cells: A review. J. Mater. Sci.: Mater. Electron. **35**(3), 226 (2024)
Purushotham, S., Ramkumar, G., Kannan, V., Kumar, A.: Simulation of thin insulating tunnel layer for Cu2ZnSnS4/CdS interface passivation. Phys. Scr. **98**(12), 125951 (2023)
Saadat, M., Amiri, O., Rahdar, A.: Optimization of (Zn, Sn) O buffer layer in Cu (in, Ga) Se2 based solar cells. Sol. Energy. **189**, 464–470 (2019)
Sekar, K., Marasamy, L., Mayarambakam, S., Hawashin, H., Nour, M., Bouclé, J.: Lead-free, formamidinium germanium-antimony halide (FA 4 GeSbCl 12) double perovskite solar cells: The effects of band offsets. RSC Adv. **13**(36), 25483–25496 (2023)
Shoab, M., Aslam, Z., Zulfequar, M., Khan, F.: Numerical interface optimization of lead-free perovskite solar cells (CH3NH3SnI3) for 30% photo-conversion efficiency using SCAPS-1D. Next Mater. **4**, 100200 (2024)
Vanalakar, S.A., Patil, P.S., Kim, J.H.: Recent advances in synthesis of Cu2FeSnS4 materials for solar cell applications: A review. Sol. Energy Mater. Sol. Cells. **182**, 204–219 (2018)
Verma, M., Routray, S.R., Mishra, G.P.: Analysis and optimization of BSF layer for highly efficient GaInP single junction solar cell, *Materials Today: Proceedings*, vol. 43, pp. 3420–3423, (2021)
Vu, T.V., et al.: A theoretical and experimental study of the valence-band electronic structure and optical constants of quaternary copper mercury tin sulfide, Cu2HgSnS4, a potential material for optoelectronics and solar cells. Opt. Mater. **96**, 109296 (2019)
Wang, J., Azam, W.: Natural resource scarcity, fossil fuel energy consumption, and total greenhouse gas emissions in top emitting countries. Geosci. Front. **15**(2), 101757 (2024)
Wang, D., Zhao, W., Zhang, Y., Liu, S.F.: Path towards high-efficient kesterite solar cells. J. Energy Chem. **27**(4), 1040–1053 (2018)
Wang, W., et al.: Over 6% certified Sb2 (S, Se) 3 solar cells fabricated via in situ hydrothermal growth and postselenization. Adv. Electron. Mater. **5**(2), 1800683 (2019)
Wang, D., et al.: Tuning the work function of the metal back contact toward efficient Cu2ZnSnSe4 solar cells. Solar RRL. **5**(1), 2000391 (2021)
Wei, Y., Tang, B., Liang, X., Zhang, F., Tang, Y.: An Ultrahigh-Mass-Loading Integrated Free-Standing Functional All-Carbon positive electrode prepared using an Architecture Tailoring Strategy for High-Energy-Density Dual-Ion batteries. Adv. Mater. **35**(30), 2302086 (2023)
Xian, K.J., et al.: Optimizing Photovoltaic Performance in CZTS-Based zn (1 – x) sn x O (x = 0.100, 0.133, 0.167, 0.200 and 0.233) thin Film Solar cells: A structural, morphological and optical study. Arab. J. Sci. Eng., pp. 1–18, (2023)
Yadav, A., Patel, A.K., Mishra, R.: Modeling and Simulation of CZTS Solar cell using Zn1-xMgxO as a buffer layer and cul as a hole transport layer for efficiency improvement. Eng. Res. Express. **6**(1), 015031 (2024)
Zhang, J., et al.: Enhanced efficiency with CDCA co-adsorption for dye-sensitized solar cells based on metallosalophen complexes. Sol. Energy. **209**, 316–324 (2020)
Zhang, C., et al.: Micro-mechanism study of the effect of Cd-free buffer layers ZnXO (X = Mg/Sn) on the performance of flexible Cu2ZnSn (S, Se) 4 solar cell. Chin. Phys. B. **32**(2), 028801 (2023)
Zhu, C.: Optimizing and using AI to study of the cross-section of finned tubes for nanofluid-conveying in solar panel cooling with phase change materials. Eng. Anal. Boundary Elem. **157**, 71–81 (2023)
Zhu, C., et al.: Optimizing solar-driven multi-generation systems: A cascade heat recovery approach for power, cooling, and freshwater production. Appl. Therm. Eng. **240**, 122214 (2024)

Authors and Affiliations

Baseerat Bibi[1] · Tauseef Anwar[2] · Ahmad M. Saeedi[3] · Raed H. Althomali[4] · Gideon F. B. Solre[5] · Sadia Malik[6] · Fatma A. Ibrahim[7] · Mohamed S. Hamdy[7] · Sana Ullah Asif[8] · Waseem Ur Rahman[9] · Saqlain Haider[10]

✉ Sana Ullah Asif
sanaullahasif@gmail.com

✉ Waseem Ur Rahman
engr.waseem778@gmail.com

[1] School of Physics and Astronomy, Yunnan University, Kunming 650091, P.R. China

[2] Department of Physics, Division of Science and Technology, University of Education Lahore, Lahore, Pakistan

[3] Department of Physics, Faculty of Science, Umm AL-Qura University, Makkah 24382, Saudi Arabia

[4] Department of Chemistry, College of Science and Humanities in Al-Kharj, Prince Sattam Bin Abdulaziz University, Al-Kharj 11942, Saudi Arabia

[5] Department of Chemistry, Thomas J. R. Faulkner College of Science, Technology, Environment, and Climate Change, University of Liberia, Monrovia, Montserrado County 00231, Liberia

[6] Department of Physics, Govt. Sadiq College Women University Bahawalpur, Bahawalpur 63100, Pakistan

[7] Catalysis Research Group (CRG), Department of Chemistry, College of Science, King Khalid University, P.O. Box 9004, Abha 61413, Saudi Arabia

[8] School of Materials and Energy, Yunnan University, Kunming 650091, P. R. China

[9] School of Mechanical Engineering, Dalian University of Technology, Dalian, China

[10] Institute of Physics, Bahauddin Zakariya University Multan, Multan, Pakistan